SCIENCE CHINA
Information Sciences

• RESEARCH PAPER •

April 2025, Vol. 68, Iss. 4, 140403:1–140403:6
https://doi.org/10.1007/s11432-024-4092-3

Special Topic: Photonics Technology

β-Ga_2O_3 solar-blind ultraviolet light detector with infinite PDCR

Haifeng CHEN[1*], Xu ZHAO[1], Xiangtai LIU[1], Qin LU[1], Shaoqing WANG[1], Zhan WANG[1], Yifan JIA[1], Yunhe GUAN[1], Lijun LI[1] & Yue HAO[2]

[1]*Key Laboratory of Advanced Semiconductor Devices and Materials, School of Electronic Engineering, Xi'an University of Posts and Telecommunications, Xi'an 710121, China*
[2]*State Key Discipline Laboratory of Wide Band Gap Semiconductor Technology, School of Microelectronics, Xidian University, Xi'an 710071, China*

Received 13 March 2024/Revised 29 April 2024/Accepted 1 July 2024/Published online 4 March 2025

Abstract Ultra-high photo-dark current ratio (PDCR) has always been a fascinating indicator for photodetectors. In this paper, the β-Ga_2O_3 solar-blind ultraviolet (UV) light detector with Ni-Ni double Schottky-junctions structure is prepared. The detector has an ultra-high PDCR value exceeding 10^8 under 254 nm UV light irradiation. The physical mechanism behind this phenomenon is to control the current competition between the two Schottky junctions by setting the drain voltage V_d and the source voltage V_s. When the flowing direction of the current in the device is converted, the current balance point B at which the dark current $I_{d(dark)}$ is zero appears during the conversion. Theoretically, at B point, PDCR should be infinite if the photo-current $I_{d(photo)}$ is not 0. In the experiment, B point where $I_{d(dark)}$ is actually 0 is obtained at $V_d = 10.1$ V in the V_d-I_d curve under $V_s = 20$ V and $I_{d(photo)}$ at B point is 8.52 μA, so the infinite PDCR realizes at B point. This paper provides new insight into Ga_2O_3 solar blind UV detectors.

Keywords Ga_2O_3, PDCR, Schottky junction, solar-blind ultraviolet, photodetector

Citation Chen H F, Zhao X, Liu X T, et al. β-Ga_2O_3 solar-blind ultraviolet light detector with infinite PDCR. Sci China Inf Sci, 2025, 68(4): 140403, https://doi.org/10.1007/s11432-024-4092-3

1 Introduction

Solar-blind ultraviolet (SUV) light detectors have many applications in military and civil fields. β-Ga_2O_3 is an ultra-wide bandgap semiconductor material, and its bandgap is about 4.5–4.9 eV, which makes it a natural preferred material for SUV detectors. Recently, research in the field has become increasingly active, and researchers have continuously reported detectors with excellent indicators and new records. Among the indicators of these detectors, photo-dark current ratio (PDCR) is very critical, which reflects the response characteristics of the device to UV light. In 2016, Oh et al. used graphene electrodes to prepare an SUV detector based on a stripped β-Ga_2O_3 sheet. It was found that, under the 254 nm UV illumination, the detector had an ultra-high PDCR of 1.18×10^6 [1]. In 2019, Han et al. prepared an amorphous Ga_2O_3 thin film transistor by chemical etching. The device had a high photocurrent I_{photo} of about 10^{-4} A and a low dark current I_{dark} of 10^{-12} A, and its PDCR is as ultra-high as 5×10^7 [2]. Kim et al. fabricated a phototransistor based on the stripped β-Ga_2O_3 material using graphene as a highly transparent gate. Its PDCR is particularly excellent, which reaches up to 6.0×10^8 [3]. In 2020, Zhang et al. prepared UV detectors based on the β-Ga_2O_3 thin films grown by pulsed laser deposition. At 20 V, I_{dark} was only 100 fA, and I_{photo} could reach 16 μA, and the maximum PDCR also reached 10^8 [4]. In 2021, Qin et al. deposited α-Ga_2O_3 thin films by magnetron sputtering, and annealed them in N_2 atmosphere at 400°C. The PDCR of SUV detector prepared by this method reaches 3.9×10^7 [5]. In 2022, Han et al reported an InGaZnO/α-Ga_2O_3 double active layer TFT. Under the illumination of 254 nm UV light, the device has a PDCR of 10^8 as well [6].

Theoretically, PDCR depends on I_{photo} and I_{dark}, and I_{photo} generally can not be increased indefinitely, so the devices with ultra-high PDCR in the above research are generally heavily dependent on ultra-low

* Corresponding author (email: chenhaifeng@xupt.edu.cn)

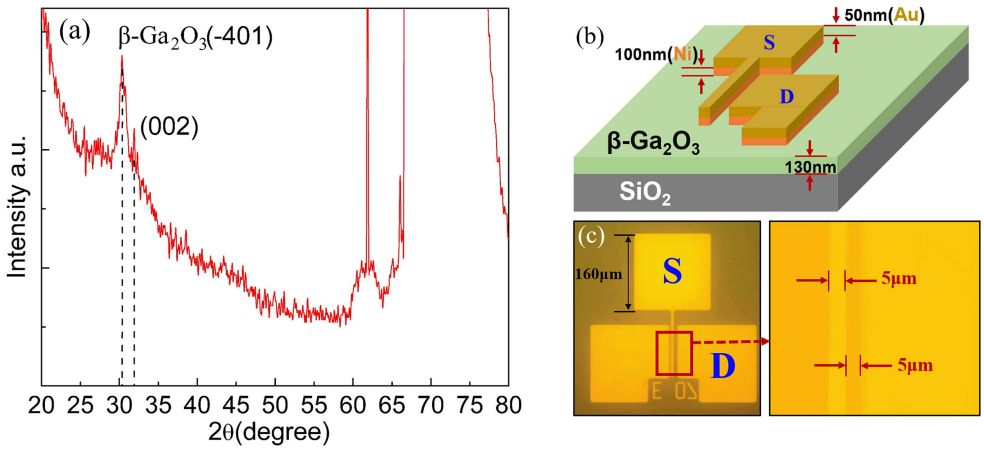

Figure 1 (Color online) (a) XRD pattern of Ga_2O_3 thin films grown by ALD; (b) schematic diagram of device structure; (c) images of prepared Ni-Ni double Schottky-junctions structure device.

I_{dark}. The control of I_{dark} is one of the keys for detectors to realize ultra-high PDCR [7–9]. Then, an interesting and serious question should be raised: What is the boundary of the minimum dark current and could it be zero?

In this paper, Ga_2O_3 thin films are grown on SiO_2/Si substrate based on Atomic Layer Deposition (ALD), and then Ni-Ni double Schottky-junctions device is prepared on the thin films. The current characteristics of the device under the dark and UV light illumination conditions are studied, and the physical mechanism of obtaining the minimum I_{dark} is discussed in order to answer and verify the above question.

2 Experiments

Ga_2O_3 thin films with 130 nm thickness were grown on a SiO_2/Si substrate by ALD, and annealed at 900°C [10]. In Figure 1(a) the XRD pattern shows the grown material after annealing is β-Ga_2O_3 with only two crystal orientations of (-401) and (002). Among them, (-401) is the main crystal orientation. The few impurity peaks indicate that the crystal quality of the material is good [11]. Then, the Ni/Au pads with a thickness of 100/50 nm were deposited on the β-Ga_2O_3 thin film to form electrodes of source S and drain D by using lithography and electron beam evaporation processes, as shown in Figure 1(b). Figure 1(c) is the image of the prepared Ni-Ni double Schottky-junctions device. The main area of electrodes is about 160 μm × 160 μm and the distance between S and D electrodes is 5 μm. For the measurement of drain current I_d, the drain voltage V_d was swept from −10 V to 20 V at the fixed source voltage V_s. All current-voltage (I-V) curves of devices were tested by keysight B1505A semiconductor parameter analyzer at room temperature under dark condition and 254 nm UV light with an intensity of 1800 μW/cm^2.

3 Results and discussion

The Ni/Au electrodes at S and D regions deposited on β-Ga_2O_3 form two back-to-back Schottky junctions, as shown in the upper part of Figure 2(a). The Fermi levels of S and D are respectively E_{FMS} and E_{FMD}, and the Fermi level of β-Ga_2O_3 is E_{FN}. The relative differences between E_{FMS} and E_{FMD} can be created by applying different voltages on S and D, and E_{FN} is generally located between them. These three Fermi levels couple with each other. The electrons located at E_{FMS} and E_{FMD} should occupy E_{FN} [12–16]. Their occupation probabilities are expressed by f_S and f_D, respectively:

$$f_S = f(E_{FN} - E_{FMS}) = \frac{1}{1 + \exp[(E_{FN} - E_{FMS})/kT]}, \tag{1}$$

$$f_D = f(E_{FN} - E_{FMD}) = \frac{1}{1 + \exp[(E_{FN} - E_{FMD})/kT]}, \tag{2}$$

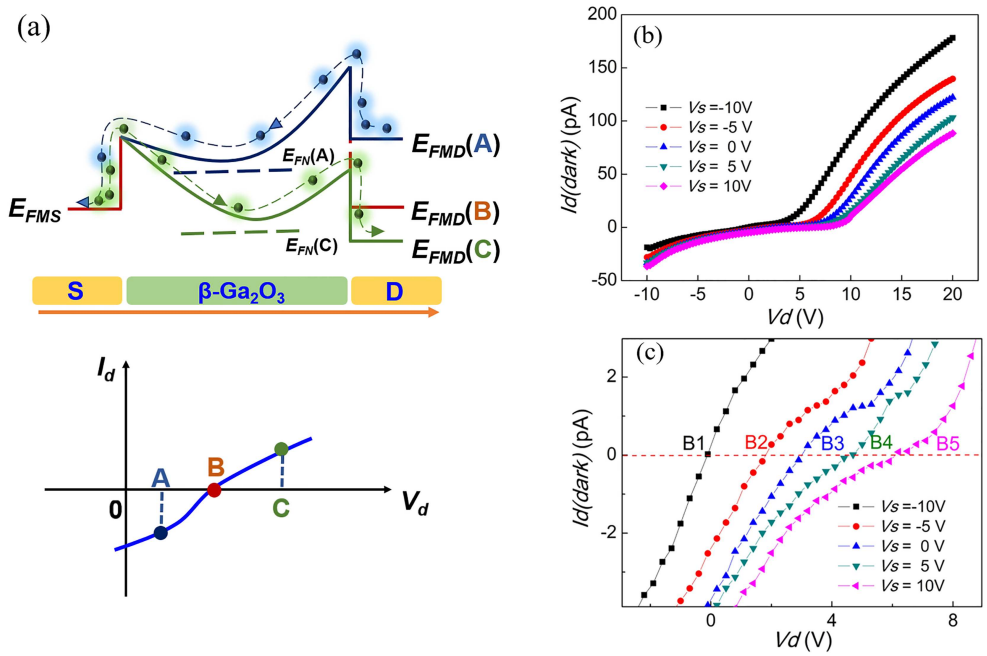

Figure 2 (Color online) (a) Schematic diagram of energy bands for current commutation process; (b) experimental $I_{d(dark)}$-V_d curves at different V_s; (c) changes of the balance point B of $I_{d(dark)}$ curves of (b) at different V_s.

where k, T are Boltzmann's constant and temperature, respectively. Therefore, the total drain current I_d of the electrons in the device flowing from S to D should be proportional to the difference between f_S and f_D:

$$I_d \propto (f_S - f_D). \tag{3}$$

In the upper part of Figure 2(a), E_{FMD}(A), E_{FMD}(B), and E_{FMD}(C) are the three locations of E_{FMD}. They are defined as greater than, equal to, and less than E_{FNS}, respectively. According to Eqs. (1)–(3), for the case of $E_{FMS} = E_{FMD}$(B), theoretically no current flows and $I_d = 0$. When E_{FMD} is at E_{FMD}(A), $f_S < f_D$ and electrons flow from D to S, resulting in a negative I_d. The opposite situation is that $f_S > f_D$ when $E_{FMS} < E_{FMD}$(C). In this case, the electron flows from S to D, and I_d is positive [17–21]. Based on the above discussion, we can achieve current reversal in devices by manipulating the relative positions of E_{FMS} and E_{FMD}. V_d and V_s can control this type of relative positions, thereby determining f_S and f_D. As shown in the bottom part of Figure 2(a), I_d will be switched from negative to positive as V_d increases from A to C point which corresponds to E_{FMD}(A) and E_{FMD}(C). In this process, there must be a switching point with $I_d = 0$, which is the balance point B corresponding to E_{FMD}(B) [22,23]. Figure 2(b) is the experimental I_d-V_d curves in dark environment. Under different fixed V_s, V_d is swept from −10 V to 20 V, and it is found that I_d truly increases from negative to positive. Figure 2(c) is an enlarged view of Figure 2(b) near the B point under different V_s, which shows that B shifts rightwards from B_1 to B_5 as V_s increases from −10, −5, 0 and 5 V to 10 V.

Furthermore, under 254 nm UV light irradiation, the photo-generated carriers increase greatly [24–26]. As shown in Figure 3(a), E_{FN} increases to $E_{FN(pho)}$ under UV light illumination due to the accumulation of photo-generated electrons. At this time, the Schottky-junction at D is more forwards biased than that under dark condition, so a large number of photo-generated electrons enter the drain region and the photo current $I_{d(photo)}$ increases greatly [27–31]. Figure 3(b) shows the experimental $I_{d(photo)}$-V_d curves. It can be seen that $I_{d(photo)}$ changes from negative to positive as V_d increases, and point B is located at the voltage where the positive and negative currents switch. This experimental result shows that the above mechanism still holds on under illumination. Figure 3(c) extracts V_d corresponding to B point at different V_s before and after illumination from Figure 2(c) and Figure 3(b). As can be seen from Figure 3(c), these V_d(B), V_d at point B, before and after illumination are linear with V_s, and their slopes are 0.306 and 0.828, respectively. In Figure 3(c), changes of V_d(B) during irradiation are divided into I($V_s <$ 5 V) and II($V_s >$ 5 V) cases, which correspond to the decrease and increase of V_d(B), respectively. In I case, V_d(B) under illumination decreases, that is to say, $I_{d(photo)@I}$ curve shifts to the left, causing its

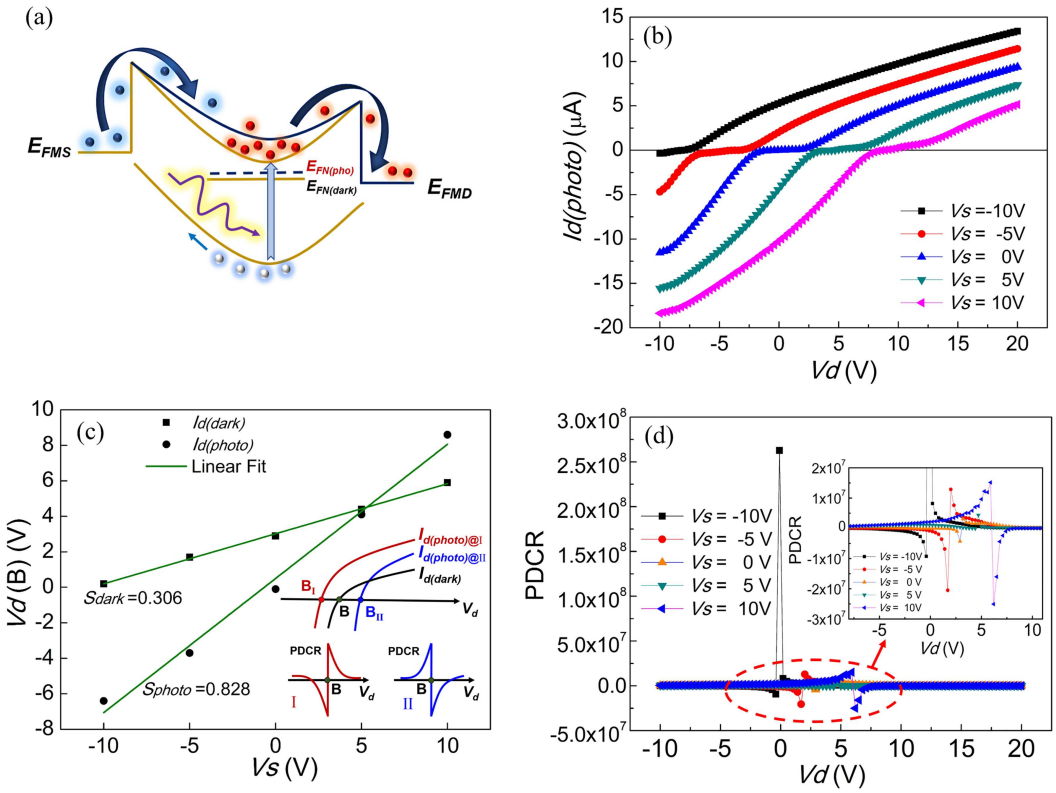

Figure 3 (Color online) (a) Schematic diagram of energy band under 1800 μW/cm^2 UV irradiation; (b) current characteristics measured at different V_s under 254 nm UV irradiation; (c) V_d(B)-V_s curves of light and dark current extracted from Figure 3(b) and Figure 2(c). The inset is the illustration of two types of PDCR; (d) PDCR-V_d curves at different V_s.

point B to drift to the left B_I point, as shown in the inset of Figure 3(c). As V_s decreases, the difference of V_d(B) before and after illumination begins to expand. When V_s = 5 V, they are very close. When $V_s > 5$ V, V_d(B) after illumination exceeds that before illumination, which is shown in the II case.

PDCR is as follows:

$$\text{PDCR} = I_{d(\text{photo})}/I_{d(dark)}. \tag{4}$$

According to Eq. (4), because $I_{d(dark)}$ at B point is zero, the PDCR peak should appear here and be infinite in theory. The illustrations of PDCR in the I and II cases are further shown in the inset of Figure 3(c). The PDCR peak around B point in I case is first negative and then positive as increasing V_d. The situation of II case is just the opposite, positive first and then negative. Figure 3(d) shows the PDCR curves extracted from the experimental I_d-V_d curves in Figures 2(b) and 3(b). Note that the PDCR peaks are more than 10^7 near point B, regardless of positive or negative V_s. When V_s= −10 V, the positive PDCR peak is more than 2.5 × 10^8. The experimental results verify the above principles, but PDCR is not infinite. This is because $I_{d(dark)}$ near point B was adopted in the experiment due to test voltage sampling and it is not I_{dark} at real B point. There is still a very small deviation between them.

Next, it is necessary to find out the real point B that can reach 0 A in the experiment. Figure 4(a) shows the experimental I_d-V_d curve under the dark and UV condition when V_s = 20 V. The inset of Figure 4(a) shows that $I_{d(dark)}$ is exactly 0 A at V_d = 10.1 V, which is its real point B. In addition, the B point in the case of UV, shifts rightwards. Figure 4(b) shows the PDCR ratio of Figure 4(a), and the PDCR increases to 4.4 × 10^7 when V_d increases from −5 V to 9.8 V. When V_d = 10.4 V, PDCR is −1.18 × 10^8. However, $I_{d(dark)}$ = 0 A and $I_{d(photo)}$ = −8.52 × 10^{-6} A when V_d = 10.1 V. As a result, its PDCR is infinite, as can be seen in Figure 4(b). In fact, the physical mechanism guarantees that every experimental $I_{d(dark)}$ curve will have a real B point. During the measurement, the current curve is made up of a large number of V_d sampling points. Sometimes there is a small deviation at point B in the test, which is due to too few sampling points or too large sampling interval. So, if one wants to get the B point where the current is very close to zero value or actually zero value, increasing the number of

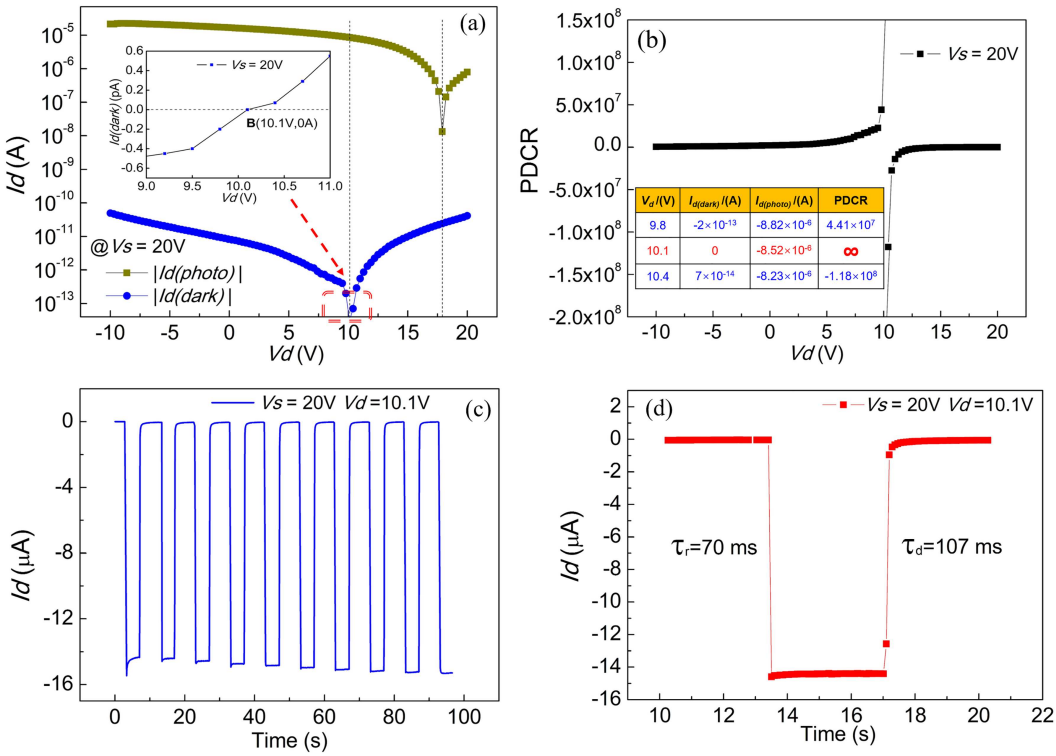

Figure 4 (Color online) (a) Light and dark currents of $V_s = 20$ V in semilogarithmic coordinates. The inset shows the experimental point B of $I_{d(dark)} = 0$ A in linear coordinates; (b) infinite PDCR at B point based on the result of (a). The table shows the PDCR data near point B; (c) I_d-T curves at point B; (d) the rising time and decline time of I-T curve.

sampling points and decreasing the sampling interval should be an effective way. Figure 4(c) presents the I-T curve at this time under the 254 nm UV light illumination, which is uniform and consistent. Figure 4(d) further shows the rising and falling times are very short and they are 70 ms and 107 ms, respectively. This experimental result reflects that the device has good UV light response characteristics.

4 Conclusion

In this paper, the solar-blind UV light detector of β-Ga_2O_3 with Ni-Ni double Schottky junctions is studied. The device can control the flow direction of current inside the device by setting V_d and V_s, thus forming the current balance point B which is zero in theory. Therefore, PDCR at point B under illumination will be extremely large. The experimental results show that V_s range from -10, -5, 0, 5 V to 10 V, and their maximum PDCR under these settings can be beyond 10^8. Furthermore, when V_s is 20 V, the real point B with $I_d = 0$ A is found in the experiment. At this point, the device obtains infinite PDCR at point B. The I-T curve at this B point obtained shows good optical turn-off characteristics, and the rising and falling times are very short, 70 ms and 107 ms respectively. The physical mechanism behind this result is to control the flowing direction of current in device, which makes it work in a wide range. So the infinite PDCR should also occur for double Schottky-junctions structure photodetector based on other photosensitive materials, electrode materials, and electrode shapes as long as there the flowing direction of current can be converted. The results will provide a new method for high PDCR of Ga_2O_3 SUV light sensors and can be used to resist the effect of SUV light on Ga_2O_3 if the focus is on point B of photocurrent.

Acknowledgements This work was supported by Natural Science Basic Research Program of Shaanxi Province of China (Grant No. 2023-JC-YB-574) and National Natural Science Foundation of China (Grant No. 62304178).

References

1 Oh S, Kim C K, Kim J. High responsivity β-Ga_2O_3 metal semiconductor metal solar-blind photodetectors with ultraviolet transparent graphene electrodes. Acs Photonics, 2017, 5: 1123–1128
2 Han Z, Liang H, Huo W, et al. Boosted UV photodetection performance in chemically etched amorphous Ga_2O_3 thin-film transistors. Adv Opt Mater, 2020, 8: 1901833

3 Kim S, Oh S, Kim J. Ultrahigh deep-UV sensitivity in graphene-gated β-Ga_2O_3 phototransistors. ACS Photonics, 2019, 6: 1026–1032
4 Zhang X, Wang L, Wang X, et al. High-performance β-Ga_2O_3 thickness-dependent solar blind photodetector. Opt Express, 2020, 28: 4169–4177
5 Qin Y, Li L H, Yu Z A, et al. Ultra-high performance amorphous Ga_2O_3 photodetector arrays for solar-blind imaging. Adv Sci, 2021, 8: 2101106
6 Han Z Y, Song S, Liang H L, et al. High-performance IGZO/Ga_2O_3 dual-active-layer thin film transistor for deep UV detection. Appl Phys Lett, 2022, 120: 262102
7 Fu S, Wang Y, Han Y, et al. β-Ga_2O_3-based solar-blind photodetector with ultrahigh responsivity via optimizing interdigital electrode parameters. IEEE Electron Device Letters, 2022, 43: 1511–1514
8 Wu C, Zhao T, He H, et al. Enhanced performance of Gallium-based wide bandgap oxide semiconductor heterojunction photodetector for solar-blind optical communication via oxygen vacancy electrical activity modulation. Adv Opt Mater, 2024, 12: 2302294
9 Tong L, Su C, Li H, et al. Self-driven Gr/WSe_2/Gr photodetector with high performance based on asymmetric Schottky van der Waals contacts. ACS Appl Mater Interf, 2023, 15: 57868–57878
10 Alema F, Hertog B, Mukhopadhyay P, et al. Solar blind Schottky photodiode based on an MOCVD-grown homoepitaxial β-Ga_2O_3 thin film. APL Materials, 2019, 7: 022527
11 Zhang X, Wang L, Wang X, et al. High-performance β-Ga_2O_3 thickness dependent solar blind photodetector. Opt Express, 2020, 28: 4169–4177
12 Arora K, Goel N, Kumar M, et al. Ultrahigh performance of self-powered β-Ga_2O_3 thin film solar-blind photodetector grown on cost-effective Si substrate using high-temperature seed layer. ACS Photonics, 2018, 5: 2391–2401
13 Latreche A. Conduction mechanisms of the reverse leakage current of β-Ga_2O_3 Schottky barrier diodes. Semicon Phys Quantum Electron Optoelectron, 2019, 22: 397–403
14 Zun X L, Shi Q Y, Wen X M, et al. A high responsivity and photosensitivity self-powered UV photodetector constructed by the CuZnS/Ga_2O_3 heterojunction. Adv Mater Interf, 2022, 10: 2202130
15 Zhang Z, Tan P, Hou X, et al. Breaking the responsivity-speed dilemma of α-GaO_x photodetector by alternating gate modulation. Sci China Inf Sci, 2023, 66: 229408
16 Han Z, Liang H, Huo W, et al. Boosted UV photodetection performance in chemically etched amorphous Ga_2O_3 thin-film transistors. Advanced Optical Materials, 2020, 8: 1901833
17 Huo N, Konstantatos G. Recent progress and future prospects of 2D-based photodetectors. Adv Mater, 2018, 30: 1801164
18 Ma J, Fang C, Chen C, et al. Chiral 2D perovskites with a high degree of circularly polarized photoluminescence. ACS Nano, 2019, 13: 3659–3665
19 Li J, Chen X, Qiao Z, et al. Large-scale synthesis of single-crystalline β-Ga_2O_3 nanoribbons, nanosheets and nanowires. J Phys Conden Matter, 2001, 13: 937–941
20 Chen X, Ren F, Ye J, et al. Review of gallium-oxide-based solar-blind ultraviolet photodetectors. Photonics Research, 2019, 7: 381–415
21 Shihyun A, Fan R, Janghyuk K, et al. Effect of front and back gates on β-Ga_2O_3 nano-belt field-effect transistors. Appl Phys Lett, 2016, 109: 062102
22 Zhong M, Wei Z, Meng X, et al. High-performance single crystalline UV photodetectors of β-Ga_2O_3. J Alloy Compound, 2015, 619: 572–575
23 Qin Y, Dong H, Long S B, et al. Enhancement-mode β-Ga_2O_3 metal-oxide-semiconductor field-effect solar-blind phototransistor with ultrahigh detectivity and photo-to-dark current ratio. IEEE Photonics Technol Lett, 2019, 40: 742–745
24 Lv Y, Wang Y, Fu X, et al. Demonstration of β-Ga_2O_3 junction barrier Schottky diodes with a Baliga's figure of merit of 0.85 GW/cm^2 or a 5 A/700 V handling capabilities. IEEE Trans Power Electron, 2020, 36: 6179–6182
25 Kim J, Tadjer M, Mastro M, et al. Controlling the threshold voltage of β-Ga_2O_3 field-effect transistors via remote fluorine plasma treatment. J Mater Chemistry C, 2019, 7: 8855–8860
26 Yuan J, Wu C, Wang S, et al. Enhancing plasticity in optoelectronic artificial synapses: A pathway to efficient neuromorphic computing. Appl Phys Lett, 2024, 124: 021101
27 Zhang Q, Deng J, Li R, et al. Study on the structural, optical and electrical properties of N-doped Ga_2O_3 films synthesized by sol-gel method. Mater Sci Semicon Process, 2024, 170: 107955
28 Yuan Y, Li Z, Hou X, et al. Enhancing the performance of β-Ga_2O_3 solar-blind photodetectors based on $ZnGa_2O_4$ substrate by bottom-up Zn diffusion doping. J Alloy Compound, 2023, 969: 171596
29 He H, Wu C, Hu H, et al. Bandgap engineering and oxygen vacancy defect electroactivity inhibition in highly crystalline N-alloyed Ga_2O_3 films through plasma-enhanced technology. J Phys Chem Lett, 2023, 14: 6444–6450
30 Varshney U, Sharma A, Goswami L, et al. Deep ultraviolet-visible highly responsivity self-powered photodetector based on β-Ga_2O_3/GaN heterostructure. Vacuum, 2023, 217: 112570
31 Li Z, Xu Y, Zhang J, et al. Flexible solar-blind Ga_2O_3 ultraviolet photodetectors with high responsivity and photo-to-dark current ratio. IEEE Photon Journal, 2019, 11: 1–9